Mettl14-mediated m^{6}A modification ensures the cell cycle progression of late-born retinal progenitor cells

Liang Li[1], Yue Sun[1,2], Alexander E. Davis[1], Man-Ru Wu[1], Cheng-Hui Lin[1], Sui Wang[1*]

Affiliations:

[1] Department of Ophthalmology, Mary M. and Sash A. Spencer Center for Vision Research, Byers Eye Institute, Stanford University, Stanford, CA 94304, USA

[2] Department of Neurosurgery, Stanford University, Stanford, CA 94305, USA

***Please send correspondence to**:

Sui Wang

suiwang@stanford.edu

Key words: Mettl14, m^{6}A mRNA methylation, Epitranscriptomic regulation, retinal progenitor cells (RPCs), cell cycle, retinal development, Zfp292

Abstract

Neural progenitor cells lengthen their cell cycle to prime themselves for differentiation as development proceeds. It is currently not clear how they counter this lengthening and avoid being halted in the cell cycle. Here, we show that m^6A (N^6-methyladenosine) methylation of cell cycle-related mRNAs ensures the proper cell cycle progression of late-born retinal progenitor cells (RPCs), which are born towards the end of retinogenesis and have long cell cycle durations. Conditional deletion of *Mettl14*, which is required for depositing m^6A on mRNAs, significantly reduced the level of m^6A modification in the developing mouse retina. This led to cell cycle arrest and subsequent cell death of late-born RPCs, but appeared to have no effect on early-born RPCs. M^6A-seq, which maps m^6A modified mRNAs, and single cell transcriptomic analyses revealed that mRNAs involved in promoting cell cycle arrest were highly enriched for m^6A modification, which targeted them for degradation and guaranteed proper cell cycle progression of late-born RPCs. In addition, we identified *Zfp292* as a novel target of m^6A and potent inhibitor of RPC cell cycle progression. Overall, our work establishes m^6A modification as an important mechanism countering cell cycle lengthening in late-born neural progenitor cells.

Introduction

During central nervous system (CNS) development, the cell cycle progression and differentiation of neural progenitor cells are precisely coordinated (Hardwick and Philpott 2014; Hardwick et al. 2015; Homem et al. 2015; Miles and Tropepe 2016; Belmonte-Mateos and Pujades 2022). One of the common observations across different cell lineages is that neural progenitor cells lengthen their cell cycles as development proceeds, which was found to be necessary for accumulating differentiation related factors (Hardwick and Philpott 2014; Miles and Tropepe 2016). While studies have focused on understanding cell cycle lengthening and its association with differentiation, it is not clear how neural progenitors counter the lengthening and avoid being halted within the cell cycle for an extended time. An improved understanding of how neural progenitor cells control cell cycle progression has broad implications and can benefit cancer and regeneration-based studies.

The neural retina is a highly advantageous model for studying the cell cycle progression of neural progenitor cells. Access to retinal progenitor cells (RPCs) using techniques such as in vivo electroporation and gamma-retrovirus based lineage tracing provides a strong platform for studying RPC cell cycle progression and differentiation (Matsuda and Cepko 2007; Turner and Cepko 1987). The length of the RPC cell cycle increases during retinal development from approximately 14 hours at embryonic day 14 (E14) to about 30 hours at neonatal stages in rodent models (Alexiades and Cepko 1996). This cell cycle lengthening coincides with RPCs transitioning from early-born RPCs that differentiate into early-born neurons, such as ganglion cells and cones, to late-born RPCs that adopt late-born cell fates, including bipolar interneurons and Müller glial cells (Cepko

et al. 1996). While the exact mechanisms controlling the lengthening of the RPC cell cycle have yet to be elucidated, cell cycle components, including cyclin, CDK and CDK inhibitors, transcription factors, such as Vsx2, Pax6, Meis1/2 and Six3/6, epigenetic regulators, and differentiation related genes all play important roles (Miles and Tropepe 2016). RPCs must counteract this cell cycle lengthening to ensure proper cell cycle progression and avoid being halted in the cell cycle. However, not much is known about the mechanisms that deter cell cycle lengthening, which is especially relevant to late-born RPCs with extended cell cycle duration.

Post-transcriptional m^6A (N^6-methyladenosine) modification is the most common internal modification on eukaryotic mRNAs and has been shown to play important roles in numerous biological processes, including neural development (Yu et al. 2021). It regulates many aspects of mRNA metabolism, including stability, translation, splicing and nuclear export (Jiang et al. 2021). m^6A is deposited by the “writer” complex, which contains the core components Mettl3 (Methyltransferase like-3), Mettl14 (Methyltransferase like-14) and WTAP (Wilms Tumor 1-Associating Protein) (Yang et al. 2018). Deleting either *Mettl3* or *Mettl14* can deplete m^6A. Yoon et al. 2017 showed that m^6A depletion resulted in a prolonged cell cycle in neural stem cells in the cerebral cortex and extended neurogenesis in postnatal stages in *Mettl14$^{f/f}$;Nestin-Cre* mice. Using the same animal model, Wang et al. 2018 reported that depletion of m^6A in neural stem cells led to decreased proliferation and premature differentiation in the cortex. Even though additional studies are needed to explain the discrepancy, these studies strongly support the importance of m^6A in neural progenitor cells and encouraged us to examine the function of m^6A using RPC as a model system.

Here we show that m^{6}A methylation on mRNAs is a key mechanism that enables late-born RPCs to counter cell cycle lengthening. We conditionally deleted *Mettl14* in RPCs from the beginning of retinogenesis and found that m^{6}A modification ensures proper cell cycle progression of late-born RPCs.

Results

Late-born retinal progenitor cells (RPCs) fail to exit cell cycle on time with *Mettl14* deletion

The genes involved in regulating m^{6}A dynamics are robustly expressed in the developing retina as revealed by quantitative PCR (qPCR) (Fig S1A&B). We detected the METTL14 protein, a required component of the m^{6}A writer complex, in the retina starting from embryonic day 12.5 (E12.5) to adulthood in most retinal cell types (Figure 1A&S1C). To study the function of m^{6}A in the developing retina, we generated a *Mettl14* conditional knockout mice (Mettl14-cKO) by crossing *Mettl14$^{f/f}$* mice with the *Chx10-Egfp/Cre* mouse line, which expresses EGFP and Cre simultaneously starting from approximately E13.5 in RPCs (Figure S1D) (Rowan and Cepko 2004). The Mettl14 protein and total m^{6}A methylation levels were significantly lower in Mettl14-cKO retinas compared to controls (Wildtype, *Mettl14$^{f/f}$*, *Mettl14$^{f/+}$* or *Mettl14$^{f/+}$;Chx10-Egfp/Cre* mice), demonstrating successful depletion of Mettl14-mediated m^{6}A modification in the retina (Figure 1A&S1D-E).

Mettl14-cKO mice showed significantly decreased eyeball size and retinal thickness compared to those of controls at postnatal day 21 (P21), when retinal development had just completed in mice (Figure 1B-C&S1F), indicating defective

developmental processes. At P7, the outer plexiform layer (OPL) was well formed in control retinas but almost absent in Mettl14-cKO retinas (Figure 1B). This was further confirmed by the absence of Bassoon expression, which is a well-established marker for ribbon synapses residing in the OPL (Figure 1D) (Dick et al. 2003). Accompanied by this delayed formation of the OPL, we observed a significant number of cells expressing the cell cycle marker Ki67 in the central and mid-peripheral areas of Mettl14-cKO retinas at P7, while Ki67+ cells were rarely found in controls in these areas at this stage (Figure 1E). We further showed that these Ki67+ cells in P7 Mettl14-cKO mice incorporated the thymidine analog EdU (5-ethynyl-2´-deoxyuridine), which labels cells in the S phase of the cell cycle (Fig 1F&G) (Buck et al. 2008). These results demonstrate that RPCs fail to exit the cell cycles by P7 in the absence of *Mettl14*.

Interestingly, we did not observe any significant defects in Mettl14-cKO retinas at or prior to birth. At P0, the retinal thickness and the number of RPCs were not significantly different between Mettl14-cKO and control retinas (Figure S2A-C). No obvious developmental defects were detected at embryonic stages in Mettl14-cKO retinas (Figure S1D-F). Mettl14-mediated m^6A modification appears to be dispensable for early retinal development.

We then deleted the *Mettl14* gene in RPCs starting from P0 by in vivo electroporation to further investigate the role of *Mettl14* in late-born RPCs (refer to the RPCs that were born after birth in this manuscript). Electroporation primarily targets mitotic RPCs because nuclear envelope breakdown is necessary for plasmids to enter nuclei (Matsuda and Cepko 2007, 2004). We co-electroporated the *CAG-Cre* and *CAG-LoxP-stop-LoxP-GFP* plasmids into P0 *Mettl14*$^{f/f}$ mouse retinas in vivo (Figure S2G). The

retinal cells expressing Cre contained *Mettl14* deletion and were highlighted by GFP expression. The *Mettl14*$^{f/f}$ retinas received *CAG-GFP* plasmids were served as controls. At P7, we observed significantly increased number of Ki67+ cells in the electroporated part of the retina in the presence of Cre, but not in the retinas received control plasmids (Figure S2G). This phenocopies Mettl14-cKO retinas and further confirms that *Mettl14* is required for late-born RPCs to exit the cell cycle.

Mettl14-depleted late-born RPCs are arrested in cell cycle and largely undergo cell death

To further investigate how *Mettl14* depletion affects late-born RPCs, we traced the abnormal RPCs found at P7 in Mettl14-cKO retinas using EdU pulse-chase assays. We injected EdU into Mettl14-cKO and control mice at P7 and harvested the retinas at P8, P9, P10 or P14. Retinal development progresses from the central to peripheral regions (Venters et al. 2015). Cell differentiation has finished in the central and mid-peripheral regions of the retina by P7 in wildtype mice. We did not observe any EdU+ cells in these regions in control mice at or after P7 (Figure 1G). In Mettl14-cKO retinas, a significant number of EdU+ cells were found at P8 (24 hours after EdU injection) and P9 (48 hours after EdU injection). Notably, the number of EdU+ cells did not increase at P9 compared to P8 (Figure 2B). Given that the duration of the RPC cell cycle is estimated to be ~30 hours (Alexiades and Cepko 1996), this suggests that EdU+ P7 RPCs did not divide in Mettl14-cKO retinas. Interestingly, most of these EdU+ cells remained Ki67+ at P8 and P9, indicating that they neither exited cell cycle nor underwent differentiation (Figure 2C). At P10, most of the EdU+ cells were dead in Mettl14-cKO retinas (Figure 2D&E). We

examined the fates of the few surviving EdU+ RPCs in Mettl14-cKO retinas at P14 when we can confidently measure cell fates by marker expression. We found that they had mainly differentiated into bipolar interneurons (~35%) and Müller glial cells (~36%) (Figure 2F-G). These results suggest that deletion of *Mettl14* and depletion of Mettl14-mediated m^6A induces late-born RPC cell cycle arrest and subsequent cell death. The small fraction of surviving cells is biased towards adopting late-born cell fates compared to wild type P2 and P5 RPCs (Figure S3A).

We further confirmed our findings by examining the P0 RPCs in control and Mettl14-cKO retinas. At P0, it is difficult to trace RPC division and fates by EdU pulse-chase assays due to the large number of proliferating RPCs and the high but partial penetrance of the *Chx10-Egfp/Cre* line (Rowan and Cepko 2004). We therefore used replication-incompetent-gamma-retrovirus-based lineage tracing analyses to study P0 RPCs in control and Mettl14-cKO mice. LIA retroviruses, which only sparsely integrate into mitotic RPCs and drive reporter gene expression in all progeny cells, are commonly used for lineage tracing studies in the retina (Turner and Cepko 1987; Hafler et al. 2012; Wang et al. 2014). We subretinally injected LIA retroviruses expressing either alkaline phosphatase (AP) alone or Cre and AP into P0 *Mettl14*$^{f/f}$ mice, and harvested the retinas at P9, right before the occurrence of significant cell death at P10, or at P14 (Figure 2H). We quantified the size and composition of each clone that originated from a single P0 RPC. The average clone size was significantly decreased when *Mettl14* was deleted by *LIA-Cre* viruses compared to controls (Figure 2I). Consistently, the number of clones containing more than 2 cells was significantly reduced in *Mettl14*$^{f/f}$ retinas received LIA-Cre viruses (Figure 2J). Therefore, P0 *Mettl14*-deleted RPCs fail to proliferate normally

in a manner similar to abnormal P7 Mettl14-CKO RPCs. Notably, we observed a significant number of one cell clones with morphologies differing from rod, bipolar, amacrine or Müller glial cells in *Mettl14*-deleted retinas at P9 (Fig S3B). These "unidentified" cells are likely to be arrested RPCs, as we observed in P9 Mettl14-cKO retinas. At P14, the progeny cells of *Mettl14*-deleted P0 RPCs also favored the bipolar and Müller glial fates (Figure S3C).

Overall, these results suggest that late-born RPCs are cell cycle-arrested in the absence of *Mettl14*. These arrested RPCs primarily undergo cell death, and the surviving cells favor late-born bipolar and Müller glial fates.

m^{6}A directly regulates cell cycle-related genes in the developing retina

To investigate the molecular mechanisms underlying *Mettl14*-depletion-induced late-born RPC cell cycle arrest, we profiled m^{6}A modified mRNAs in the developing retina at P7 and searched for mRNAs whose m^{6}A levels were eliminated with *Mettl14* deletion. Methylated RNA immunoprecipitation sequencing (MeRIP-seq or m^{6}A-seq), which uses an antibody against m^{6}A to immunoprecipitate m^{6}A-enriched mRNAs, allows for mapping of m^{6}A modified mRNAs in a genome-wide manner (Delatte et al. 2016). We examined P7 control and Mettl14-cKO retinas using m^{6}A-seq in combination with regular RNA-seq.

The m^{6}A modification was found to be enriched at the consensus RRACH motif (R=G or A; H=G, A or C) in both control and Mettl14-cKO retinas at P7, which is consistent with studies in other systems (Figure 3A) (Chen et al. 2015; Zhang et al. 2019). The overall landscape of m^{6}A was not significantly changed in Mettl14-cKO, with m^{6}A modified sites primarily locating at CDS (coding DNA sequence), stop codon and 3'UTR (3'

untranslated region) (Figure 3B). In control P7 retinas, mRNAs of approximately 79% of expressed genes contained significant levels of m^6A modification (Figure 3C). These m^6A-modified mRNAs are highly enriched for involvement in pathways such as neurogenesis and stem cell differentiation (Figure 3D). Compared to controls, a total of 1269 genes were differentially expressed in Mettl14-cKO retinas. Among the 482 downregulated genes, approximately 12% of the genes showed significantly reduced m^6A levels. However, the reduction of m^6A levels showed no correlation with changes of mRNA levels (data now shown). Among the 787 significantly upregulated genes, the mRNAs of 101 genes were m^6A modified and showed significantly reduced m^6A enrichment in Mettl14-cKO retinas. For these genes, the reduction of m^6A levels was negatively correlated with changes of mRNA levels, which is consistent with the major role of m^6A modification in mediating mRNA decay (Figure 3E). We focused on these genes, hypothesizing that they are likely to be direct targets of m^6A modification. Gene Ontology analyses revealed that these genes were highly involved in cell cycle related pathways, including cell division, regulation of cell cycle process, and cellular response to DNA damage stimulus (Figure 3F). We confirmed the increased mRNA levels and stability of top candidate genes in Mettl14-cKO retinas using quantitative PCR (Figure 3G and data not shown). Whereas some of these genes are involved in promoting cell cycle progression, many are known to promote cell cycle arrest, such as *Brca2, Brip1, Foxm1, Ttk* and *Birc5* (Figure 3G) (Gudmundsdottir and Ashworth 2006; Cantor and Guillemette 2011; Zona et al. 2014; Wei et al. 2005; Lens et al. 2003). The upregulation of these genes collectively led to cell cycle arrest, as we observed in Mettl14-cKO retinas. Thus,

Mettl14 deletion-mediated m^6A depletion resulted in sustained high levels of mRNAs that can promote cell cycle arrest, which induced late-born RPC cell cycle arrest.

Single cell RNA-seq reveals molecular events downstream of m^6A modification in the developing retina

We performed single cell transcriptomic analyses (scRNA-seq via 10x Genomics) to further reveal *Mettl14* depletion-induced changes in late-born RPCs and different retinal cell types. We recovered 10451 cells from four P7 control retinas and 13116 cells from four Mettl14-cKO retinas. Based on well-established markers for retinal cell types (Clark et al. 2019), we assigned known cell identities to the 25 clusters grouped by an unbiased clustering method (Seurat 4.1) (Figure S4). The 11 RPC-derived cell types were selected for downstream analyses (Figure 4A-C). In addition to the seven major retinal cell types (rod, cone, Müller glia, bipolar, amacrine, horizontal and ganglion cells), we detected cell clusters representing RPCs and precursors of rod, Müller glia, and bipolar cells in P7 retinas. We focused on analyzing the RPC and precursor cell clusters to elucidate the mechanisms underlying m^6A regulation.

In Mettl14-cKO retinas, there were increased number of *Mki67*+ (the gene encoding Ki67) RPCs compared to controls (Fig 4C). Some *Mki67*+ cells were also found in Müller glia and bipolar cell precursor clusters in Mettl14-cKO but not in controls (Figure 4D). This increased number of *Mki67*+ cells is consistent with the observations described in Figure 1 and 2. In addition, the percentage of retinal cells differentiating towards bipolar and Müller glial fates (BP+BP-pre, MG+MG-pre) was increased in Mettl14-cKO retinas compared to controls, whereas the percentage of cells differentiating towards rod fate

(Rod+Rod-pre) was decreased. This matches our finding that surviving RPCs favor bipolar and Müller glial fates (Figure 2F&G). Notably, the proportions of the precursor cells for rod, bipolar, and Müller glial cells were all increased in Mettl14-cKO retinas, suggesting a development delay, possibly due to RPC cell cycle arrest. The proportions of the cell types derived from early-RPCs, such as ganglion cells, cones, and horizontal cells, were not changed in Mettl14-cKO retinas compared to control retinas (Figure 4C).

We analyzed the genes that were differentially expressed in the RPC cluster in control and Mettl14-cKO retinas. The cell cycle-related genes revealed by m^6A-seq and bulk RNA-seq (Figure 3G) showed increased expression in Mettl14-cKO RPCs compared to control RPCs (Figure 4E). The top 10 genes that were significantly upregulated in Mettl14-cKO RPCs were highlighted in Figure 4E and 4F. Most of these genes showed reduced m^6A levels based on m^6A-seq (Figure S5A). Some of these genes have been implicated in regulating the cell cycle in other systems(Zhou et al. 2018; Wang et al. 2019; Liang et al. 2014; Bhargava et al. 2018; Gong et al. 2021), but their roles in RPC cell cycle progression have not been well studied. The top candidate was *Zfp292*, which encodes the transcription factor Zinc Finger Protein 292 (also known as Znf292). It was highly modified by m^6A in control retinas, and its m6A level was significantly reduced in Mettl14-cKO retinas (Figure 4G & S5A). Several studies have identified *Zfp292* as a tumor suppressor gene (Takeda et al. 2015; Jh et al. 2016; Gong et al. 2021), but its function in the retina or the CNS is unknown. We over-expressed *Zfp292* in wildtype late-born RPCs and examined whether sustained expression of *Zfp292* can inhibit the cell cycle progression of late-born RPCs. The plasmid over-expressing *Zfp292* (*CAG-Zfp292*) was delivered into P0 mouse retinas *ex vivo* via electroporation. The *CAG-GFP* plasmids were

co-electroporated with the *CAG-Zfp292* plasmids to label the cells over-expressing *Zfp292*. The efficiency of co-electroporating two types of plasmids into the same cells exceeds 90% (Matsuda and Cepko 2004, 2007). Twenty-four hours after retinas were electroporated with the control or *CAG-Zfp292* plasmids, we applied EdU to retinas for 1 hour and harvested them 2, 30, or 60 hours later to trace the cell cycle progression of late-born RPCs (Figure 4H &S6). As development proceeded, the GFP+EdU+ cells gradually exited the cell cycle and became Ki67 negative. The percentage of GFP+EdU+ cells that were GFP+EdU+Ki67+ continuously decreased at 30 and 60 hours after the EdU pulse in controls, while the percentage remained high in retinas over-expressing *Zfp292*. This demonstrated that the RPCs over-expressing *Zfp292* failed to exit the cell cycle normally as development proceeded. The total number of GFP+EdU+ cells was not significantly higher when *Zfp292* was over-expressed compared to controls, suggesting that *Zfp292* did not promote RPC proliferation. Based on these results, we concluded that *Zfp292* over-expression can significantly inhibit late-born RPC cell cycle progression. The increased levels of *Zfp292* mRNAs in Mettl14-cKO retinas thus can contribute to RPC cell cycle arrest.

We also analyzed differentially expressed genes in clusters classified as precursors for rods, bipolar cells, or Müller glial cells. Interestingly, *Cdkn1a*, which encodes the $P21^{Cip1}$ protein and is well-known for its role in inhibiting cell cycle progression (Karimian et al. 2016), was significantly upregulated in all three precursor clusters in Mettl14-cKO retinas (Figure 4D&S5B-D). Notably, the *Cdkn1a* mRNAs were unlikely to be directly regulated by m^6A because m^6A-seq did not detect m^6A enrichment on *Cdkn1a* mRNAs (Figure 4I). The increased level of *Cdkn1a* is likely to be an indirect event induced by m^6A

depletion. Interestingly, while not statistically significant, *Cdkn1a* mRNA levels appeared to be higher in the RPC cluster in Mettl14-cKO retinas compared to control retinas (Figure 4D). We confirmed the increased levels of *Cdkn1a* mRNA and protein in Mettl14-cKO retinas at P7 using qPCR, *in situ* RNA hybridization, and immunofluorescent staining (Figure 4J & S5E-F). It is likely that this m^6A depletion induced $P21^{Cip1}$ upregulation also contributes to RPC cell cycle arrest and subsequent cell death in Mettl14-cKO retinas.

In addition, we compared the P7 Mettl14-cKO RPCs with wildtype P0, P2 and P8 RPCs in published scRNA-seq datasets (Figure S7A) (Clark et al. 2019). The P7 Mettl14-cKO RPCs intermingled with wildtype RPCs as shown in the UMAP (Uniform Manifold Approximation and Projection) plot, suggesting that they are not dramatically different from wildtype RPCs at the transcriptional levels (Figure S7B-E). The cell-cycle scoring and regression analyses (Seurat 4. 0. 6) revealed that the percentage of P7 Mettl14 RPCs in the G2/M phases of the cell cycle was higher than that in P7 control RPCs (Figure S7F). This indicates that Mettl14-cKO RPCs may be arrested in the G2/M phases. Notably, P7 Mettl14-cKO RPCs differentially expressed genes that are involved in the cellular senescence pathway (Figure S7G). Given that $P21^{Cip1}$ is a well-established senescence marker (Kumari and Jat 2021), this result further supports that $P21^{Cip1}$-related pathways play important roles downstream of m^6A depletion.

Taken together, the scRNA-seq analyses further confirmed our above findings and revealed *Zfp292* and *Cdkn1a* to be important contributors of m^6A depletion-induced late-born RPC cell cycle arrest.

Discussion

We investigated mechanisms countering the RPC cell cycle lengthening during retinal development. We showed that Mettl14-mediated m^6A modification is critical for ensuring the proper cell cycle progression of late-born RPCs. Depletion of m^6A modification by conditionally deleting the *Mettl14* gene in the developing retina led to cell cycle arrest and subsequent cell death of late-born RPCs. m^6A-seq and scRNA-seq revealed that mRNAs involved in promoting cell cycle arrest were highly enriched for m^6A, and their levels were significantly higher in the absence of *Mettl14* in late-born RPCs. In addition, we identified *Zfp292* to be a novel target of m^6A in the developing retina and showed that $P21^{Cip1}$-related pathways were involved in mediating the cell cycle arrest induced by m^6A depletion. Notably, m^6A modification appeared to be dispensable for RPCs that were born before birth, because no significant defects were detected in the retina prior to or at birth. Based on these results, we propose a model for how late-born RPCs counter the cell cycle lengthening during retinal development (Figure 5). Under wildtype conditions, the mRNAs inhibiting cell cycle progression, such as *Zfp292*, are modified by m^6A, which decreases their mRNA levels and can avoid uncontrolled cell cycle arrest. In the absence of m^6A, these mRNAs are more stable, resulting in cell cycle arrest and the subsequent cell death of late-born RPCs.

While it has not been studied in the developing retina, the function of m^6A modification on neural development has been reported. During cortical neurogenesis, depletion of m^6A via deleting different components of the m^6A machinery resulted in two major outcomes. First, a prolonged cell cycle of embryonic neural progenitor cells and extended neurogenesis were found in *Mettl14* or *Fmr1* (encodes a protein reading m^6A and mediating mRNA nuclear export) conditional knock out mice (Yoon et al. 2017; Edens

et al. 2019). Second, deletion of *Mettl14* or *Ythdf2* (encoding a protein reading m^{6}A and primarily mediating mRNA decay) resulted in reduced proliferation and premature differentiation of neural progenitor cells (Wang et al. 2018; Li et al. 2018). During cerebellar development, m^{6}A modification downregulated apoptosis-related mRNAs and ensured the survival of newly generated cerebellar granule cells (Wang et al. 2018a). Here we show that m^{6}A down regulates mRNAs that promote cell cycle arrest and ensures the proper cell cycle progression of late-born RPCs in the developing retina. Therefore, m^{6}A can regulate distinct cellular processes in different neural progenitor cell types, possibly via targeting different mRNAs in a context-dependent manner.

One of the unique findings of the present study is that m^{6}A regulation is required in late-born RPCs but appeared to be dispensable for early-born RPCs. While intensively studied, our understanding of the heterogeneity and competence of RPCs is still limited. Recent single cell transcriptomic analyses revealed that there are clearly two distinct populations of RPCs, which are the ones born before or after E16-E18 (Clark et al. 2019). Our work shows that RPCs born after birth (late-born RPCs) are sensitive to m^{6}A regulation, and further highlights the heterogeneity among RPCs.

This study also identified a novel target of m^{6}A in the developing retina, *Zfp292*, which can significantly inhibit the cell cycle progression of late-born RPCs. However, overexpression of *Zfp292* alone is not sufficient to fully recapitulate the phenotypes observed in Mettl14-cKO retinas. For instance, we did not detect Ki67+ cells in the central and mid-peripheral retina at P7 when *Zfp292* was overexpressed in late-born RPCs in vivo (data not shown). The cell cycle arrest and subsequent cell death of late-born RPCs are likely induced by multiple genes and pathways. We further showed that *Cdkn1a*

mRNAs and proteins ($P21^{Cip1}$) were significantly upregulated in the retina upon m^6A depletion. $P21^{Cip1}$ is well-known for its role in promoting cell cycle arrest. The upregulation of $P21^{Cip1}$ does not seem to be a direct effect of m^6A depletion, because *Cdkn1a* mRNAs are not highly enriched for m^6A modification. In addition, this increased expression of $P21^{Cip1}$ is not directly downstream of *Zfp292* in that over-expression of *Zfp292* did not lead to upregulation of *Cdkn1a* in wild type retinas (data not shown). One possibility is that $P21^{Cip1}$ expression is induced or accompanied by the upregulation of genes involved in the DNA damage response pathways, which were found to be modified by m^6A and their levels were significantly increased in Mettl14-cKO retinas (Figure 3G). Most of these genes are known to promote cell cycle arrest during DNA damage repair. We did not detect obvious DNA damage in Mettl14-cKO retinas at neonatal stages (data not shown). The upregulation of these genes is likely a direct effect of m^6A depletion. Thus, it is possible that late-born RPCs express genes involved in DNA damage response pathways to prime themselves for potential DNA damage during proliferation. m^6A could be one of the mechanisms that is used by late-born RPCs to balance the levels of these genes and ensure normal cell cycle progression.

In summary, we studied how late-born RPCs counter cell cycle lengthening and ensure proper cell cycle progression. We showed that post-transcriptional m^6A modification on mRNAs plays a key role in this process. In the future, it will be important to elucidate how cell cycle duration is differentially regulated in early and late RPCs, how cell cycle lengthening is coordinated with the differentiation program, and how m^6A regulation interacts with these programs to guarantee proper development. It will also be interesting to further investigate the function of *Zfp292* during retinal development and

examine whether it can serve as a therapeutic target to control cell cycle progression under disease conditions.

Experimental procedures

Animals

The Mettl14$^{f/f}$ mouse line was a gift from Dr. Chuan He at the University of Chicago (Yoon et al. 2017). The Chx10-EGFP/Cre mice were purchased from the Jackson Lab (Stock# 005105). Wild-type mouse neonates were obtained from timed pregnant CD1 mice (Charles River Laboratories, #022). All animal studies were approved by the Administrative Panel on Laboratory Animal Care (APLAC) at Stanford University.

Plasmid Construction

The *CAG-GFP, CAG-LoxP-Stop-LoxP-GFP, CAG-Cre* and *CAG-filler* plasmids were from Wang et al. 2014. To generate the *CAG-Zfp292* plasmid, we split the mouse *Zfp292* ORF into four overlapping DNA fragments (each about ~2kb), which were then synthesized by IDT. We cloned these fragments into the *CAG-GFP* backbone by Gibson Assembly (NEB, Cat.No. E2611). Primers are listed in Table S1&2.

Western blot

Mouse retinas were freshly dissected out, transferred to RIPA buffer (Radioimmunoprecipitation assay buffer, Abcam #ab156034), and heated at 95°C for 10 mins. Protein concentrations were measured by BCA protein kit (Pierce™ BCA Protein Assay Kit #23228). Equal amounts of proteins were loaded onto a 4%-20% SDS-PAGE gel (BIO-RAD , #4561094) and run at 130V and 30A for 1.5 hours. The gel was transferred to a 0.2mm PVDF membrane (BIO-RAD, #1704156) using a semi-dry transfer system (BIO-RAD, 1704150EDU). The membrane was blocked with 5% non-fat milk blocking solution and incubated with primary antibodies at 4°C overnight. Primary antibodies included rabbit anti-Mettl14 (Sigma-Aldrich, HPA038002 1:1000) and rabbit anti-GAPDH (Abcam, ab9485, 1:1000). The membrane was washed with 1X TBST (20mM Tris,

150mM NaCl, 0.1% Tween20) for 30 mins and incubated with secondary antibody conjugated to horseradish peroxidase (Amersham, NA934-100U, 1:5000) at room temperature for 2 hours. The membrane was washed again and incubated with the SuperSignal West Pico PLUS chemiluminescent substrate mix (Thermo Scientific, #34580). Chemiluminescent signals were detected using the Amersham ImageQuant 600 (Cytiva) imaging system.

Quantitative real time PCR

Total RNA was isolated from retinal tissues using QIAGEN RNeasy kit (QIAGEN, 74104). The cDNA was generated using SuperScript™ III First-Strand Synthesis Kit (Invitrogen, 18080051). qPCR primers were listed in Table S1. The SYBR™ Green Master Mix (Fisher Scientific, A25742) was used for qPCR. The qPCR experiments were performed using a Quantstudio3 Real-Time PCR System (Applied Biosystems, A28567) with the following conditions: 50°C for 2 mins, 95°C for 10 mins, followed by 40 cycles of 95°C for 15s, 60°C for 1min.

Ex vivo and in vivo plasmid electroporation into the retina

Ex vivo and in vivo retina electroporations were carried out as previously described (Matsuda and Cepko 2004, 2007; Wang et al. 2014; Emerson and Cepko 2011). For ex vivo electroporation, 5 pulses of 25V, 50ms each with 950ms intervals were applied to dissected retinas. For in vivo electroporation, 5 pulses of 80V, 50ms each with 950ms intervals were applied to neonatal mouse pups. All ex vivo and in vivo electroporation experiments were repeated with at least three biological replicates. Plasmids were electroporated with a concentration of 500ng/ul to 1ug/ul per plasmid.

Histology and immunofluorescence

Mouse eyeballs were fixed in 4% paraformaldehyde (PFA) in 1×PBS (pH 7.4) for 2 hours at room temperature. Retinas were then dissected out and equilibrated at room temperature in a series of sucrose solutions (5% sucrose in 1× PBS, 5 min; 15% sucrose in 1× PBS, 15 min; 30% sucrose in 1× PBS, 1 h; 1:1 mixed solution of OCT and 30% sucrose in PBS, 4°C, overnight), embedded in OCT and stored at −80°C. A Leica

CM3050S cryostat (Leica Microsystems) was used to prepare 20 μm cryosections. Retinal cryosections were washed in 1× PBS briefly, incubated in 0.2% Triton, 1× PBS for 20 min, and blocked for 30 min in blocking solution (0.1% Triton, 1% BSA and 10% donkey serum in 1x PBS, Jackson Immuno Research Laboratories). Slides were incubated with primary antibodies diluted in blocking solution in a humidified chamber at 4°C overnight. After washing in 0.1% Triton 1× PBS for three times, slides were incubated with secondary antibodies and DAPI (Sigma-Aldrich; D9542) for 1 hour, then washed for three times with 0.1% Triton, 1× PBS and mounted in Fluoromount-G (Southern Biotechnology Associates). The following primary antibodies were used: chicken anti-GFP (Abcam, ab13970, 1:1000), rabbit anti-Sox9 (Abcam, ab185966, 1:500), rabbit anti-Pax6 (Thermo Fisher Scientific, 42-6600, 1:500), mouse anti-Rhodopsin (Abcam, ab5417, 1:200), mouse anti-Bassoon (Abcam, ab82958, 1:200), mouse anti-Ki67 (BD Biosciences, 550609, 1:200), and rabbit anti-P21 (1:500, Abcam, ab188224).

Retrovirus preparation and delivery in the retina

The *LIA-Cre* and *LIA* plasmids were gifts from Dr. Connie Cepko (Harvard Medical School, Boston, MA, USA). Retrovirus were packaged using HEK293T cells (ATCC-CRL-3216) and purified using ultracentrifuge following published protocols (Turner and Cepko 1987). Briefly, the *CAG-VSVG*, *CAG-gagpol*, and *LIA-Cre* or *LIA* plasmids were transfected into HEK293T cells with PEI (polyethylenimine, MW 40,000, 24765-1). Cell culture medium was replaced by 10%Nus+DMEM 24 hours after transfection. The medium was collected at 48- and 72-hour post-transfection. The medium was filtered through 0.45 mm filters (Corning, 430768) and then concentrated by ultracentrifugation (16,500 rpm, 90min). 0.5-1μl of LIA-AP/LIA-Cre (3X10^^{7} CFU/ml) viruses were delivered into the sub-retinal space of postnatal day 0 (P0) mice as previously described (Wang et al. 2014). Retinas were harvested and dissected out at P9 or P14, fixed in 4% paraformaldehyde, and stained for alkaline phosphatase activity (AP) using X-phos/NBT kit (FieldsBerry et al., 1992). After embedding in OCT (VWR, 25608-930), retinas were cryo-sectioned at 20 mm thickness and imaged under the Keyence microscope (BZ-800E).

TUNEL assay

TUNEL Assay was performed using the Click-iT™ Plus TUNEL Assay for In Situ Apoptosis Detection, Alexa Fluor™ 647 dye kit (Invitrogen™ C10619).

EdU pulse-chase assay

EdU (2.5mg/ml) was injected intraperitoneally into mice pups (50 µl/g body weight) at P7. EdU signals were detected on retinal cryosections using the EdU Cell Proliferation Kit (Invitrogen, C10340).

M^6A dot-blot assay

Total RNA samples were denatured at 95°C, spotted onto Hybond-N+ membrane (Catalog No. GERPN1510B; GE Healthcare) and crosslinked using a Stratalinker 2400 UV crosslinker. Membranes were blocked with 5% milk blocking solution for 1 hour, and then incubated with anti-m^6A antibody for 2 hours at room temperature. Membranes were washed and incubated with HRP-conjugated secondary antibodies for 1 hour at room temperature. For signal detection, membrane was incubated with ECL Western Blotting Substrate for 5 min in darkness at room temperature and then imaged using the Amersham ImageQuant 600 (Cytiva) imaging system.

RNA in situ hybridization

RNA in situ hybridization was performed using the Yn-situ method (Wu et al. 2022). Briefly, the retinal cryo-sections were fixed with 4% PFA for 1 hour, followed by EDC (1-Ethyl-3-(3-dimethylaminopropyl) carbodiimide) treatment for 1 hour at room temperature. For hybridization, sections were digested with proteinase K (1:200 dilution) at 40°C for 30 mins and blocked with hybridization buffer for 5 min. Probe mixtures were added onto the sections, which were incubated at 40°C for overnight. Slides were washed for three times with wash buffer (30% formamide, 5× SSC, 9 mM citric acid (pH 6.0), 0.1% Tween 20, 50 µg/mL heparin) and 5x SSCT (saline-sodium citrate, 0.1% Tween 20) and incubated in preamplifier (20 ng/µL) for 2 hours at 40°C. Signals were amplified by HCR hairpins (3uM) and imaged by the Zeiss confocal microscope (LSM880). Probes information can be found in Table S1.

Imaging and analysis

All images of retinal sections were acquired by a Zeiss LSM880 inverted confocal microscope. Images in Figure 1, 2, and 4 were maximum projections of 5-10μm tissues and were quantified by Fiji software.

m^6A-seq (MeRIP-seq) and data analysis

Total RNA was extracted from retina tissues using RNeasy Mini Kit (QIAGEN, 74104). Approximately 30ug of total RNA per sample with RIN number >8.0 was used for m^6A-seq. The poly(A) mRNAs were isolated by using the Dynabeads Oligo(dT) kit (ThermoFisher, #61002), fragmented into ~100bp-long oligonucleotides using divalent cations under elevated temperature, and incubated with m^6A antibody (No. 202003, Synaptic Systems, Germany) in IP buffer (50 mM Tris-HCl, 750 mM NaCl and 0.5% Igepal CA-630) supplemented with BSA (0.5 μg μl−1) for 2 hours at 4°C. The mixture was then incubated with protein-A beads and eluted with elution buffer (1 × IP buffer and 6.7mM m6A). Eluted RNAs were precipitated by 75% ethanol. Eluted m6A-containing fragments (IP) and untreated input control fragments are converted to cDNA libraries and submitted for next generation sequencing (LC-BIO Bio-tech ltd, Hangzhou, China). The sequencing quality was verified by using FastQC. Bowtie was used to map the reads to the Mus musculus (Version: v96) genome with default parameters. Mapped reads of IP and input libraries were provided for R package exomePeak to identify m^6A peaks adapted for visualization on the UCSC genome browser or IGV software. Motifs were identified and localized by using MEME scripts (Bailey et al. 2009). Called peaks were annotated by intersection with gene architecture using ChIPseeker (Yu et al. 2015). StringTie (Pertea et al. 2015) was used to perform expression analyses for all mRNAs from input libraries by calculating FPKM (total exon fragments/mapped reads(millions)×exon length(kB)). The differentially expressed mRNAs were selected with |log2 (fold change) |>1 and p value < 0.05 by R package edgeR. GO term analysis was performed by The Gene Ontology Resource (http://geneontology.org/).

Single Cell RNA sequencing (scRNA-seq) and data analysis

Retinal tissues were dissociated as described previously (Wang et al. 2014) and loaded on a 10x Genomics Chromium controller to generate single cell Gel-Beads-in Emulsion (GEMs). Single-cell RNA-Seq libraries were prepared using the Chromium Gene Expression 3' kit v3.1 (PN-1000269). The quality of the libraries was analyzed by a 2100 Bioanalyzer (Agilent) using a high-sensitivity DNA kit (Agilent, #5067–4626). The libraries were sequenced by Illumina HiSeq4000 platform (2 x 75 paired-end reads). Single cell RNA expression matrices were generated by aligning sequencing reads to a pre-build mouse reference (mm10-2020-A) using the Cell Ranger (v.6.1.1) pipeline and loaded into R (v.4.1) for downstream analyses. We applied SoupX (Young and Behjati 2020), DoubleDecon (DePasquale et al. 2019) and DoubletFinder (McGinnis et al. 2019) to remove ambient RNA and doublets. The filtered matrices were processed with Seurat (v.4.1) for quality control, clustering and visualization using standard workflows. Briefly, genes that were detected in fewer than 5 cells, and cells with fewer than 500 genes or more than 5% reads as mitochondrial were excluded from analyses. Control and Mettle14-cKO samples were normalized by SCTransform method (Hafemeister and Satija 2019) and integrated using 3000 variable genes (*PrepSCTIntegration, FindIntegrationAnchors and IntegrateData)*. Clusters were generated based on the top 30 principal components (PCs) (*FindNeighbors* function and *FindClusters* function, resolution = 1) and visualized by t-distributed Stochastic Neighbor Embedding (tSNE). To identify the conserved markers of each cluster, we performed differential gene expression tests on each cluster versus all other clusters (*FindConservedMarkers*). Clusters were assigned to 15 major cell types by their conserved markers. Differentially expressed genes (DEGs) were identified using a Wilcoxon rank-sum test (*FindAllMarkers*) between control and Mettl14-cKO in each cell type. DEGs with |log2 (fold change)| > 1 and p value < 0.05 were selected as input for GO analysis described above. To query the P7 Mettl14-cKO RPCs on published reference datasets (Clark et al. 2019), the Unimodal UMAP projection function (*Mapquery*, Seurat 4.0.6) was used.

Statistics

The sample size (n) was determined by using G*power software (two groups, the effect size of 0.5, α error at 0.05 and power set at 0.95). Personnel were blinded during

experiments. GraphPad Prism v.9 (GraphPad) was used to perform statistical analysis. Student's t-tests (two tailed) were used with the appropriate parameters. Statistical significance was defined as a P value <0.05.

Data availability

Data have been uploaded to GEO database awaiting approval.

Acknowledgements

The members of the Wang laboratory provided valuable discussion and support for this project.

Funding and additional information

Support was provided by NIH 1R01EY03258501 (to S.W. and L.L.) and P30 (P30-EY026877) to Stanford Ophthalmology (to all authors). The content is solely the responsibility of the authors and does not necessarily represent the official views of the National Institutes of Health.

Conflict of interest

The authors declare that they have no conflicts of interest with the contents of this article.

References

Alexiades MR, Cepko C. 1996. Quantitative analysis of proliferation and cell cycle length during development of the rat retina. *Developmental Dynamics* **205**: 293–307.

Bailey TL, Boden M, Buske FA, Frith M, Grant CE, Clementi L, Ren J, Li WW, Noble WS. 2009. MEME SUITE: tools for motif discovery and searching. *Nucleic Acids Res* **37**: W202-208.

Belmonte-Mateos C, Pujades C. 2022. From Cell States to Cell Fates: How Cell Proliferation and Neuronal Differentiation Are Coordinated During Embryonic Development. *Front Neurosci* **15**: 781160.

Bhargava S, Patil V, Shah RA, Somasundaram K. 2018. IGF2 mRNA binding protein 3 (IMP3) mediated regulation of transcriptome and translatome in glioma cells. *Cancer Biology & Therapy* **19**: 42–52.

Buck SB, Bradford J, Gee KR, Agnew BJ, Clarke ST, Salic A. 2008. Detection of S-phase cell cycle progression using 5-ethynyl-2′-deoxyuridine incorporation with click chemistry, an alternative to using 5-bromo-2′-deoxyuridine antibodies. *BioTechniques* **44**: 927–929.

Cantor SB, Guillemette S. 2011. Hereditary breast cancer and the BRCA1-associated FANCJ/BACH1/BRIP1. *Future Oncol* **7**: 253–261.

Cepko CL, Austin CP, Yang X, Alexiades M, Ezzeddine D. 1996. Cell fate determination in the vertebrate retina. *Proc Natl Acad Sci U S A* **93**: 589–595.

Chen T, Hao Y-J, Zhang Y, Li M-M, Wang M, Han W, Wu Y, Lv Y, Hao J, Wang L, et al. 2015. m(6)A RNA methylation is regulated by microRNAs and promotes reprogramming to pluripotency. *Cell Stem Cell* **16**: 289–301.

Clark BS, Stein-O'Brien GL, Shiau F, Cannon GH, Davis-Marcisak E, Sherman T, Santiago CP, Hoang TV, Rajaii F, James-Esposito RE, et al. 2019. Single-Cell RNA-Seq Analysis of Retinal Development Identifies NFI Factors as Regulating Mitotic Exit and Late-Born Cell Specification. *Neuron* **102**: 1111-1126.e5.

Delatte B, Wang F, Ngoc LV, Collignon E, Bonvin E, Deplus R, Calonne E, Hassabi B, Putmans P, Awe S, et al. 2016. Transcriptome-wide distribution and function of RNA hydroxymethylcytosine. *Science* **351**: 282–285.

DePasquale EAK, Schnell DJ, Van Camp P-J, Valiente-Alandí Í, Blaxall BC, Grimes HL, Singh H, Salomonis N. 2019. DoubletDecon: Deconvoluting Doublets from Single-Cell RNA-Sequencing Data. *Cell Rep* **29**: 1718-1727.e8.

Dick O, tom Dieck S, Altrock WD, Ammermüller J, Weiler R, Garner CC, Gundelfinger ED, Brandstätter JH. 2003. The presynaptic active zone protein bassoon is essential for photoreceptor ribbon synapse formation in the retina. *Neuron* **37**: 775–786.

Edens BM, Vissers C, Su J, Arumugam S, Xu Z, Shi H, Miller N, Rojas Ringeling F, Ming G-L, He C, et al. 2019. FMRP Modulates Neural Differentiation through m6A-Dependent mRNA Nuclear Export. *Cell Rep* **28**: 845-854.e5.

Emerson MM, Cepko CL. 2011. Identificati on of a Retina-specific Otx2 Enhancer Element Active in Immature Developing Photoreceptors. *Dev Biol* **360**: 241–255.

Gong W, Xu J, Wang G, Li D, Zhan Q. 2021. ZNF292 suppresses proliferation of ESCC cells through ZNF292/SKP2/P27 signaling axis. *Chin J Cancer Res* **33**: 637–648.

Gudmundsdottir K, Ashworth A. 2006. The roles of BRCA1 and BRCA2 and associated proteins in the maintenance of genomic stability. *Oncogene* **25**: 5864–5874.

Hafemeister C, Satija R. 2019. Normalization and variance stabilization of single-cell RNA-seq data using regularized negative binomial regression. *Genome Biol* **20**: 296.

Hafler BP, Surzenko N, Beier KT, Punzo C, Trimarchi JM, Kong JH, Cepko CL. 2012. Transcription factor Olig2 defines subpopulations of retinal progenitor cells biased toward specific cell fates. *Proc Natl Acad Sci USA* **109**: 7882–7887.

Hardwick LJA, Ali FR, Azzarelli R, Philpott A. 2015. Cell cycle regulation of proliferation versus differentiation in the central nervous system. *Cell Tissue Res* **359**: 187–200.

Hardwick LJA, Philpott A. 2014. Nervous decision-making: to divide or differentiate. *Trends in Genetics* **30**: 254–261.

Homem CCF, Repic M, Knoblich JA. 2015. Proliferation control in neural stem and progenitor cells. *Nat Rev Neurosci* **16**: 647–659.

Jh L, Sy S, Ms K, Nj Y, Sh L. 2016. Frameshift mutations of a tumor suppressor gene ZNF292 in gastric and colorectal cancers with high microsatellite instability. *APMIS : acta pathologica, microbiologica, et immunologica Scandinavica* **124**. https://pubmed.ncbi.nlm.nih.gov/27150435/ (Accessed May 31, 2022).

Jiang X, Liu B, Nie Z, Duan L, Xiong Q, Jin Z, Yang C, Chen Y. 2021. The role of m6A modification in the biological functions and diseases. *Sig Transduct Target Ther* **6**: 1–16.

Karimian A, Ahmadi Y, Yousefi B. 2016. Multiple functions of p21 in cell cycle, apoptosis and transcriptional regulation after DNA damage. *DNA Repair (Amst)* **42**: 63–71.

Kumari R, Jat P. 2021. Mechanisms of Cellular Senescence: Cell Cycle Arrest and Senescence Associated Secretory Phenotype. *Front Cell Dev Biol* **9**: 645593.

Lens SMA, Wolthuis RMF, Klompmaker R, Kauw J, Agami R, Brummelkamp T, Kops G, Medema RH. 2003. Survivin is required for a sustained spindle checkpoint arrest in response to lack of tension. *EMBO J* **22**: 2934–2947.

Li M, Zhao X, Wang W, Shi H, Pan Q, Lu Z, Perez SP, Suganthan R, He C, Bjørås M, et al. 2018. Ythdf2-mediated m6A mRNA clearance modulates neural development in mice. *Genome Biology* **19**: 69.

Liang L, Haug JS, Seidel CW, Gibson MC. 2014. Functional genomic analysis of the periodic transcriptome in the developing Drosophila wing. *Dev Cell* **29**: 112–127.

Matsuda T, Cepko CL. 2007. Controlled expression of transgenes introduced by in vivo electroporation. *Proc Natl Acad Sci USA* **104**: 1027–1032.

Matsuda T, Cepko CL. 2004. Electroporation and RNA interference in the rodent retina in vivo and in vitro. *Proc Natl Acad Sci USA* **101**: 16–22.

McGinnis CS, Murrow LM, Gartner ZJ. 2019. DoubletFinder: Doublet Detection in Single-Cell RNA Sequencing Data Using Artificial Nearest Neighbors. *Cell Syst* **8**: 329-337.e4.

Miles A, Tropepe V. 2016. Coordinating progenitor cell cycle exit and differentiation in the developing vertebrate retina. *Neurogenesis (Austin)* **3**: e1161697.

Pertea M, Pertea GM, Antonescu CM, Chang T-C, Mendell JT, Salzberg SL. 2015. StringTie enables improved reconstruction of a transcriptome from RNA-seq reads. *Nat Biotechnol* **33**: 290–295.

Rowan S, Cepko CL. 2004. Genetic analysis of the homeodomain transcription factor Chx10 in the retina using a novel multifunctional BAC transgenic mouse reporter. *Developmental Biology* **271**: 388–402.

Takeda H, Wei Z, Koso H, Rust AG, Yew CCK, Mann MB, Ward JM, Adams DJ, Copeland NG, Jenkins NA. 2015. Transposon mutagenesis identifies genes and evolutionary forces driving gastrointestinal tract tumor progression. *Nat Genet* **47**: 142–150.

Turner DL, Cepko CL. 1987. A common progenitor for neurons and glia persists in rat retina late in development. *Nature* **328**: 131–136.

Venters SJ, Mikawa T, Hyer J. 2015. Early Divergence of Central and Peripheral Neural Retina Precursors During Vertebrate Eye Development. *Dev Dyn* **244**: 266–276.

Wang C-X, Cui G-S, Liu X, Xu K, Wang M, Zhang X-X, Jiang L-Y, Li A, Yang Y, Lai W-Y, et al. 2018a. METTL3-mediated m6A modification is required for cerebellar development ed. C. He. *PLoS Biol* **16**: e2004880.

Wang M, Niu W, Hu R, Wang Y, Liu Y, Liu L, Zhong J, Zhang C, You H, Zhang J, et al. 2019. POLR1D promotes colorectal cancer progression and predicts poor prognosis of patients. *Mol Carcinog* **58**: 735–748.

Wang S, Sengel C, Emerson MM, Cepko CL. 2014. A gene regulatory network controls the binary fate decision of rod and bipolar cells in the vertebrate retina. *Dev Cell* **30**: 513–527.

Wang Y, Li Y, Yue M, Wang J, Kumar S, Wechsler-Reya RJ, Zhang Z, Ogawa Y, Kellis M, Duester G, et al. 2018b. N6-methyladenosine RNA modification regulates embryonic neural stem cell self-renewal through histone modifications. *Nat Neurosci* **21**: 195–206.

Wei J-H, Chou Y-F, Ou Y-H, Yeh Y-H, Tyan S-W, Sun T-P, Shen C-Y, Shieh S-Y. 2005. TTK/hMps1 participates in the regulation of DNA damage checkpoint response by phosphorylating CHK2 on threonine 68. *J Biol Chem* **280**: 7748–7757.

Wu Y, Xu W, Ma L, Yu Z, Wang Y, Yu CR. 2022. Robust and sensitive in situ RNA detection using Yn-situ. *Cell Reports Methods* **2**: 100201.

Yang Y, Hsu PJ, Chen Y-S, Yang Y-G. 2018. Dynamic transcriptomic m6A decoration: writers, erasers, readers and functions in RNA metabolism. *Cell Res* **28**: 616–624.

Yoon K-J, Ringeling FR, Vissers C, Jacob F, Pokrass M, Jimenez-Cyrus D, Su Y, Kim N-S, Zhu Y, Zheng L, et al. 2017. Temporal Control of Mammalian Cortical Neurogenesis by m6A Methylation. *Cell* **171**: 877-889.e17.

Young MD, Behjati S. 2020. SoupX removes ambient RNA contamination from droplet-based single-cell RNA sequencing data. *Gigascience* **9**: giaa151.

Yu G, Wang L-G, He Q-Y. 2015. ChIPseeker: an R/Bioconductor package for ChIP peak annotation, comparison and visualization. *Bioinformatics* **31**: 2382–2383.

Yu J, She Y, Ji S-J. 2021. m6A Modification in Mammalian Nervous System Development, Functions, Disorders, and Injuries. *Frontiers in Cell and Developmental Biology* **9**. https://www.frontiersin.org/article/10.3389/fcell.2021.679662 (Accessed May 12, 2022).

Zhang C, Fu J, Zhou Y. 2019. A Review in Research Progress Concerning m6A Methylation and Immunoregulation. *Frontiers in Immunology* **10**. https://www.frontiersin.org/article/10.3389/fimmu.2019.00922 (Accessed May 31, 2022).

Zhou L, Fu L, Lv N, Liu J, Li Y, Chen X, Xu Q, Chen G, Pang B, Wang L, et al. 2018. Methylation-associated silencing of BASP1 contributes to leukemogenesis in t(8;21) acute myeloid leukemia. *Exp Mol Med* **50**: 1–8.

Zona S, Bella L, Burton MJ, Nestal de Moraes G, Lam EW-F. 2014. FOXM1: An emerging master regulator of DNA damage response and genotoxic agent resistance. *Biochim Biophys Acta* **1839**: 1316–1322.

Figure 1

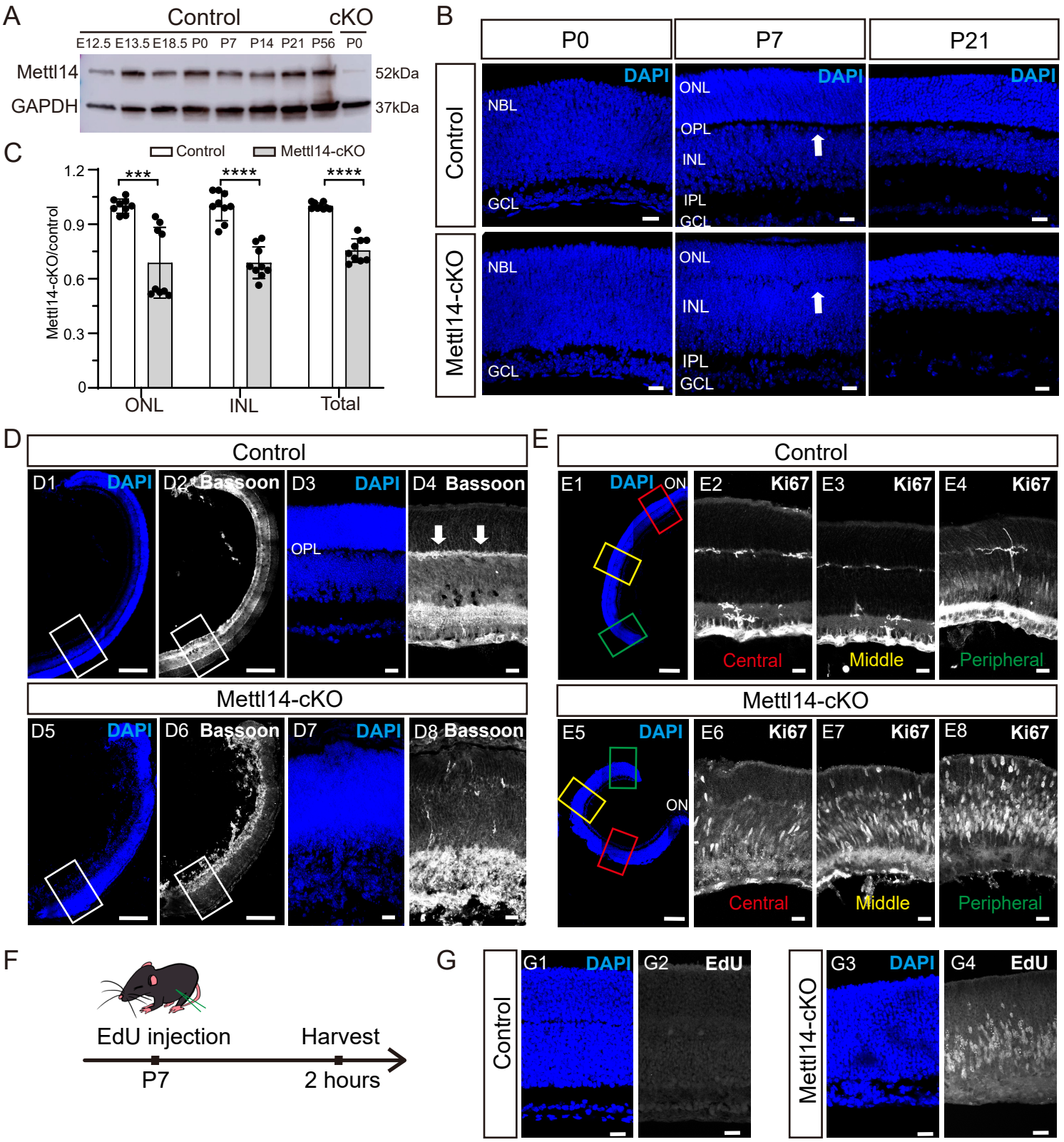
A
Control
cKO
E12.5 E13.5 E18.5 P0 P7 P14 P21 P56 P0
Mettl14
GAPDH
52kDa
37kDa
B
P0
P7
P21
Control
Mettl14-cKO
DAPI
NBL
GCL
ONL
OPL
INL
IPL
C
Control
Mettl14-cKO
Mettl14-cKO/control
1.2
0.9
0.6
0.3
0
***
****
ONL
INL
Total
D
Control
Mettl14-cKO
D1 DAPI
D2 Bassoon
D3 DAPI
D4 Bassoon
OPL
D5 DAPI
D6 Bassoon
D7 DAPI
D8 Bassoon
E
Control
Mettl14-cKO
E1 DAPI
ON
E2 Ki67
E3 Ki67
E4 Ki67
Central
Middle
Peripheral
E5 DAPI
E6 Ki67
E7 Ki67
E8 Ki67
F
EdU injection
Harvest
P7
2 hours
G
Control
Mettl14-cKO
G1 DAPI
G2 EdU
G3 DAPI
G4 EdU

Figure 1. **Late-born retinal progenitor cells (RPCs) fail to exit cell cycle at postnatal day 7 (P7) in Mettl14-cKO mice**

(A) The protein levels of METTL14 in control and Mettl14-cKO mouse retinas during retinal development. The METTL14 level is significantly reduced in Mettl14-cKO retinas at P0. **(B)** The gross morphology of Mettl14-cKO retinas at P0, P7 and P21. NBL: Neuroblastic layer; ONL: outer nuclear layer; OPL: outer plexiform layer; INL: inner nuclear layer; IPL: inner plexiform layer; GCL: ganglion cell layer. White arrows: underdeveloped OPL. Scale bar: 20μm. **(C)** The relative retinal thickness of Mettl14-cKO and control retinas at P21. Mean ± SD (n=9; ***P< 0.001; ****P< 0.0001; Two-tailed Student's T test). **(D)** Bassoon staining of control and Mettl14-cKO retinas at P7. White arrows: Bassoon staining in OPL. D3 & D4, or D7 &D8 are higher magnification views of the highlighted regions in D1 & D2 or D5 & D6. Scale bar: 200μm (D1, D2, D5 and D6) and 20μm (D3, D4, D7 and D8). **(E)** Ki67+ cells in the central, middle(mid-peripheral), and peripheral areas of P7 control and Mettl14-cKO retinas. E2-4 or E6-8 are higher magnification views of the highlighted regions in E1 or E6. Red box: Central retina; Yellow box: Mid-peripheral (Middle) retina; Green box: Peripheral retina. ON: optic nerve head. Scale bar: 200μm (E1 & E5) and 20μm (E2-E4 & E6-E8). **(F)** The schematic of the 2-hour EdU pulse-chase experiment. **(G)** EdU+ cells in P7 control and Mettl14-cKO retinas at 2 hours after EdU injection. Scale bar: 20μm.

Figure 2

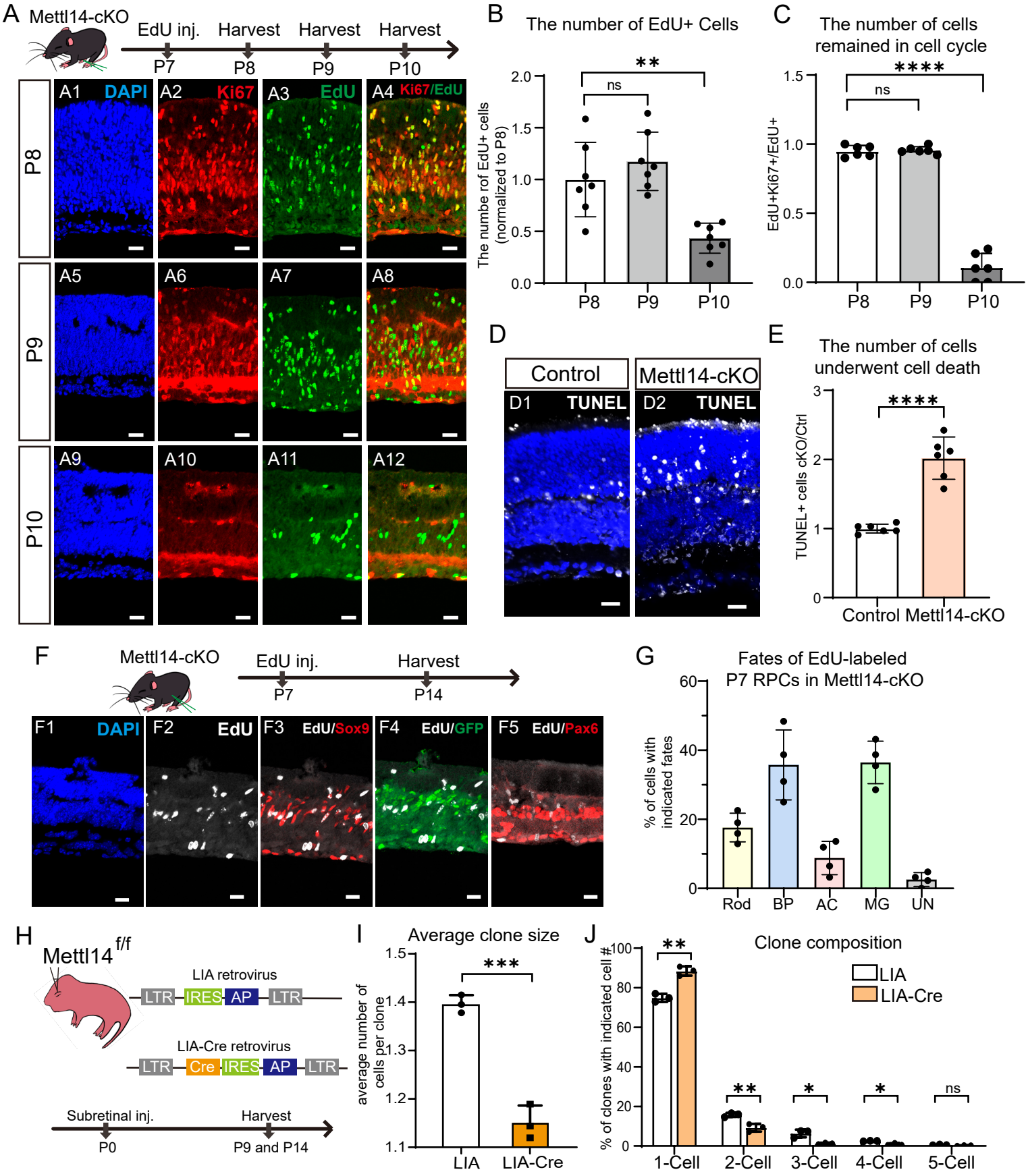
A
Mettl14-cKO
EdU inj.
Harvest
Harvest
Harvest
P7
P8
P9
P10
P8
P9
P10
A1 DAPI
A2 Ki67
A3 EdU
A4 Ki67/EdU
A5
A6
A7
A8
A9
A10
A11
A12
B
The number of EdU+ Cells
The numbe rof EdU+ cells (normalized to P8)
ns
**
P8
P9
P10
C
The number of cells remained in cell cycle
EdU+Ki67+/EdU+
ns
****
P8
P9
P10
D
Control
Mettl14-cKO
D1 TUNEL
D2 TUNEL
E
The number of cells underwent cell death
TUNEL+ cells cKO/Ctrl
****
Control
Mettl14-cKO
F
Mettl14-cKO
EdU inj.
Harvest
P7
P14
F1 DAPI
F2 EdU
F3 EdU/Sox9
F4 EdU/GFP
F5 EdU/Pax6
G
Fates of EdU-labeled P7 RPCs in Mettl14-cKO
% of cells with indicated fates
Rod
BP
AC
MG
UN
H
Mettl14 f/f
LIA retrovirus
LTR
IRES
AP
LTR
LIA-Cre retrovirus
LTR
Cre
IRES
AP
LTR
Subretinal inj.
Harvest
P0
P9 and P14
I
Average clone size
average number of cells per clone
***
LIA
LIA-Cre
J
Clone composition
% of clones with indicated cell #
LIA
LIA-Cre
**
**
*
*
ns
1-Cell
2-Cell
3-Cell
4-Cell
5-Cell

Figure 2. Mettl14-depleted late-born RPCs are arrested in cell cycle and primarily undergo cell death.

(A) Three-day EdU pulse-chase experiments in P7 Mettl14-cKO mice in vivo. The experimental design is shown on top. Scale bar: 20μm. **(B)** The number of EdU+ cells at P8, P9 and P10 in Mettl14-cKO retinas after EdU injection at P7. Data were normalized to values at P8. Mean ± SD (n=6, ** P< 0.01; Two tailed Student's T test). **(C)** The percentage of cells remained in cell cycle (Ki67+EdU+/EdU+ cells) at P8, P9 and P10 in Mettl14-cKO retinas after EdU injection at P7. Data were normalized to the values at P8. Mean ± SD (n=6, ****P< 0.0001; Two tailed Student's T test). **(D)** TUNEL+ cells in P10 control and Mettl14-cKO retinas. Scale bar: 20μm. **(E)** The number of TUNEL+ cells in P10 control and Mettl14-cKO retinas. Data were normalized to the values of the control group. Mean ± SD (n=6, ****P< 0.0001; Two tailed Student's T test). **(F)** The fates of EdU+ cells in Mettl14-cKO at P14 after EdU injection at P7. The experimental design is shown on top. Scale bar: 20μm. **(G)** The percentage of EdU+ cells that adopted indicated cell fates at P14. BP: bipolar cells; AC: amacrine cells; MG: Müller glial cells; UN: cells with unidentified fates. Mean ± SD (n=4). **(H)** The schematics of the retrovirus-based lineage tracing of P0 RPCs in Mettl14-cKO or control retinas. **(I)** The average clone size at P9. Mean ± SD (n=3, ***P< 0.001; Two tailed Student's T test). **(J)** The clone composition at P9. Mean ± SD (n=3, *P< 0.05, ** P< 0.01; Two tailed Student's T test).

Figure 3

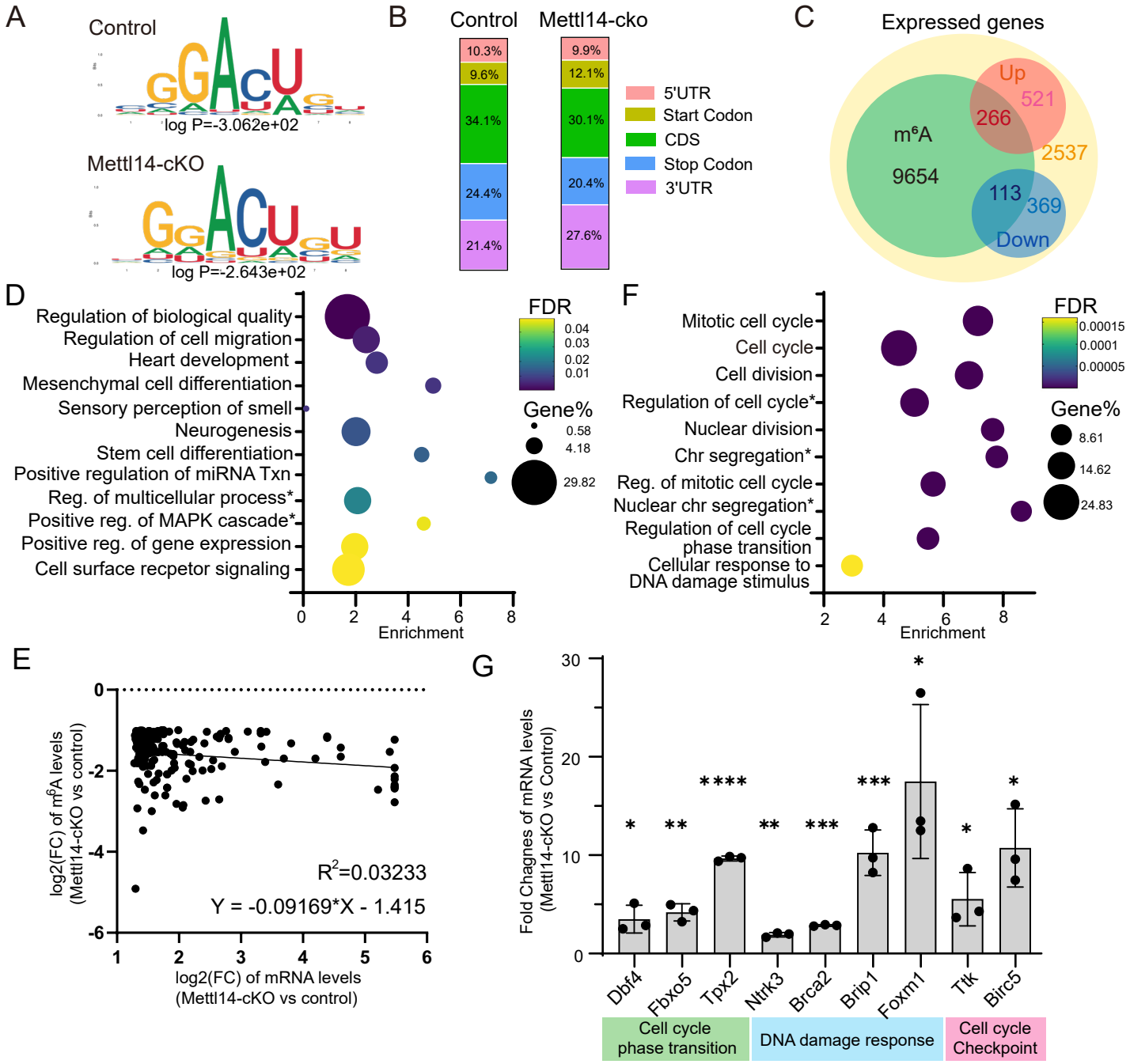
A
Control
log P=-3.062e+02
Mettl14-cKO
log P=-2.643e+02
B
Control
Mettl14-cko
10.3%
9.6%
34.1%
24.4%
21.4%
9.9%
12.1%
30.1%
20.4%
27.6%
5'UTR
Start Codon
CDS
Stop Codon
3'UTR
C
Expressed genes
m⁶A
9654
Up
521
266
2537
113
369
Down
D
Regulation of biological quality
Regulation of cell migration
Heart development
Mesenchymal cell differentiation
Sensory perception of smell
Neurogenesis
Stem cell differentiation
Positive regulation of miRNA Txn
Reg. of multicellular process*
Positive reg. of MAPK cascade*
Positive reg. of gene expression
Cell surface recpetor signaling
Enrichment
FDR
0.04
0.03
0.02
0.01
Gene%
0.58
4.18
29.82
F
Mitotic cell cycle
Cell cycle
Cell division
Regulation of cell cycle*
Nuclear division
Chr segregation*
Reg. of mitotic cell cycle
Nuclear chr segregation*
Regulation of cell cycle phase transition
Cellular response to DNA damage stimulus
Enrichment
FDR
0.00015
0.0001
0.00005
Gene%
8.61
14.62
24.83
E
log2(FC) of m⁶A levels (Mettl14-cKO vs control)
log2(FC) of mRNA levels (Mettl14-cKO vs control)
R²=0.03233
Y = -0.09169*X - 1.415
G
Fold Chagnes of mRNA levels (Mettl14-cKO vs Control)
Dbf4
Fbxo5
Tpx2
Ntrk3
Brca2
Brip1
Foxm1
Ttk
Birc5
Cell cycle phase transition
DNA damage response
Cell cycle Checkpoint

Figure 3. m^{6}A-seq reveals that m^{6}A directly regulates cell cycle related genes in the developing retina

(A) The consensus m^{6}A motifs in control and Mettl14-cKO retinas at P7. **(B)** The m^{6}A peak localization in control and Mettl14-cKO retinas at P7. **(C)** Yellow circle: the number of expressed genes in control retinas at P7. Green circle: the number of genes with m^{6}A peaks in control retinas at P7. Red circle: the number of genes that are up-regulated in Mettl14-cKO retinas at P7 compared to controls. Blue circle: the number of genes that are down-regulated in Mettl14-cKO at P7. **(D)** The GO analysis of genes that are modified by m^{6}A. **(E)** The linear regression analysis shows the correlation between m^{6}A level decrease and mRNA level increase in P7 Mettl14-cKO retinas ($P<0.05$). **(F)** The GO analysis of genes with increased mRNA levels and decreased m^{6}A levels in Mettl14-cKO retinas compared to controls at P7. **(G)** QPCR verification of top candidate genes with increased mRNA levels and decreased m^{6}A levels in Mettl14-cKO at P7. The known roles of the candidate genes are indicated in the boxes below the chart. All values were normalized to *Gapdh* levels. Data were also normalized to controls. Mean ± SD (n=3, * $P< 0.05$; ** $P< 0.01$; ***$P< 0.001$; ****$P< 0.0001$; Two tailed Student's T test).

Figure 4

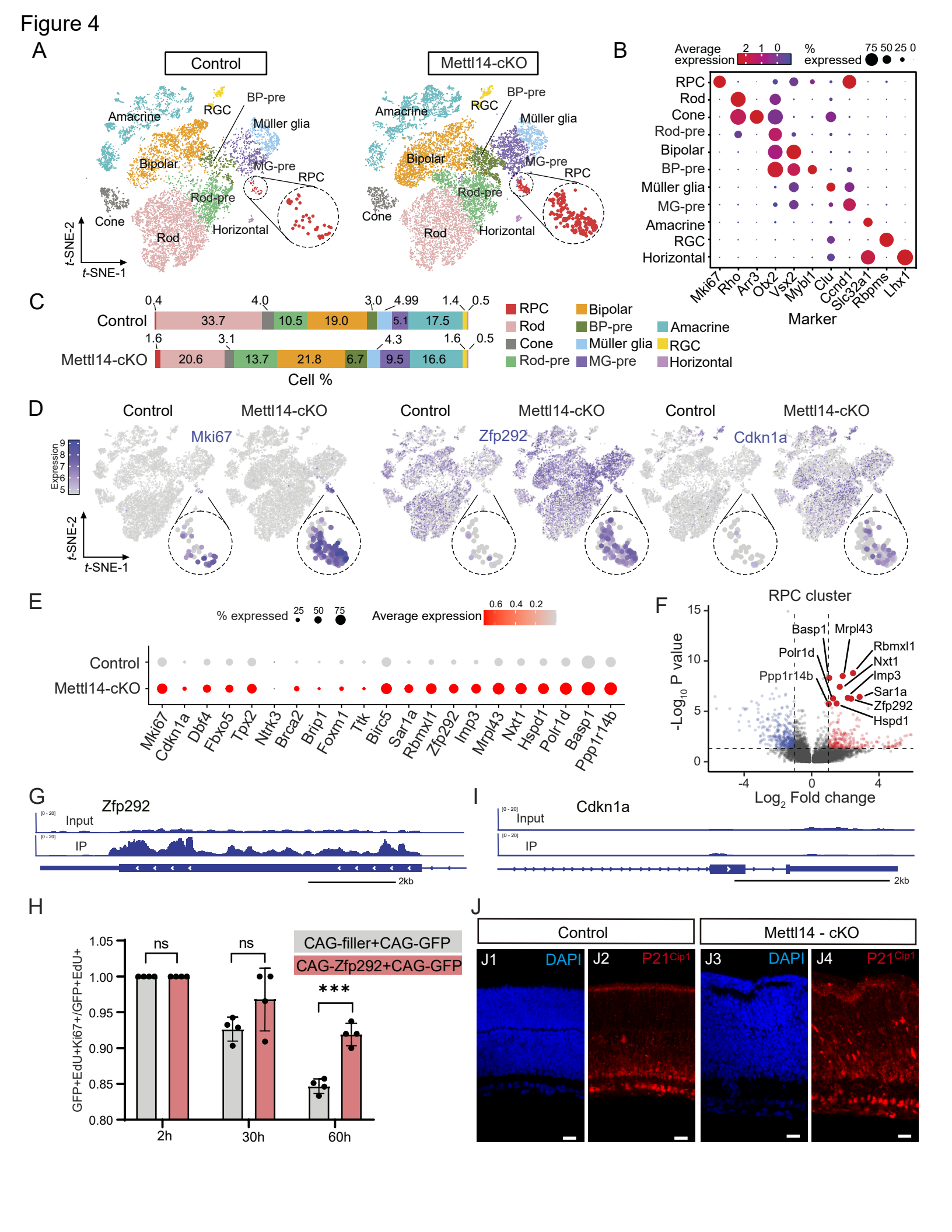
A
Control
Mettl14-cKO
Amacrine
RGC
BP-pre
Müller glia
Bipolar
MG-pre
RPC
Rod-pre
Cone
Rod
Horizontal
t-SNE-2
t-SNE-1
B
Average expression
2 1 0
% expressed
75 50 25 0
RPC
Rod
Cone
Rod-pre
Bipolar
BP-pre
Müller glia
MG-pre
Amacrine
RGC
Horizontal
Mki67
Rho
Arr3
Otx2
Vsx2
Mybl1
Clu
Ccnd1
Slc32a1
Rbpms
Lhx1
Marker
C
Control
Mettl14-cKO
0.4
33.7
4.0
10.5
19.0
3.0
4.99
5.1
17.5
1.4
0.5
1.6
20.6
3.1
13.7
21.8
6.7
4.3
9.5
16.6
1.6
0.5
Cell %
RPC
Rod
Cone
Rod-pre
Bipolar
BP-pre
Müller glia
MG-pre
Amacrine
RGC
Horizontal
D
Control
Mettl14-cKO
Mki67
Zfp292
Cdkn1a
Expression
9
8
7
6
5
t-SNE-2
t-SNE-1
E
% expressed
25
50
75
Average expression
0.6 0.4 0.2
Control
Mettl14-cKO
Mki67
Cdkn1a
Dbf4
Fbxo5
Tpx2
Ntrk3
Brca2
Brip1
Foxm1
Ttk
Birc5
Sar1a
Rbmxl1
Zfp292
Imp3
Mrpl43
Nxt1
Hspd1
Polr1d
Basp1
Ppp1r14b
F
RPC cluster
-Log10 P value
Log2 Fold change
Basp1
Mrpl43
Polr1d
Rbmxl1
Nxt1
Ppp1r14b
Imp3
Sar1a
Zfp292
Hspd1
G
Zfp292
Input
IP
2kb
I
Cdkn1a
Input
IP
2kb
H
GFP+EdU+Ki67+/GFP+EdU+
ns
ns
***
CAG-filler+CAG-GFP
CAG-Zfp292+CAG-GFP
2h
30h
60h
J
Control
Mettl14 - cKO
J1
DAPI
J2
P21Cip1
J3
DAPI
J4
P21Cip1

Figure 4. Single cell RNA-seq reveals molecular events downstream of m^6A modification in the developing retina

(A) T-SNE maps of retinal cell types captured by scRNA-seq in control (left) and Mettl14-cKO (right) retinas at P7. The cell clusters of RPCs are circled and highlighted as inserts. **(B)** Dot plot showing the markers used for identifying retinal cell types. Dot size: the proportion of cells expressing indicated marker genes. Dot color: the average expression levels. RPC: retinal progenitor cell; Rod-pre: rod precursor; BP-pre: bipolar precursor; MG-pre: Müller glia precursor; RGC: retinal ganglion cells. **(C)** The proportion of each cell cluster in control (Top) and Mettl14-cKO (Bottom) retinas at P7. **(D)** Feature plots showing the expression of *Mki67* (left), *Zfp292* (middle) and *Cdkn1a* (P21) (right) in control and Mettl14-cKO retinas at P7. The cell cluster of RPCs is circled and highlighted as inserts. **(E)** Dot plot showing the expression of cell cycle-related genes (qPCR verified in Figure 3G), and top 10 upregulated genes in RPC clusters (Mettl14-cKO vs Control). **(F)** Volcano plot showing differential expressed genes (DEGs) between Mettl14-cKO and control RPCs at P7. DEGs that are up- or down-regulated in Mettl14-cKO are illustrated in light red or blue, respectively. The cutoff for DEGs is $p < 0.05$ (Wilcoxon rank sum test) and |log2 fold change| >1 (shown as dash lines). The 10 most significantly upregulated DEGs are highlighted in red. **(G)** m^6A peaks on the *Zfp292* gene in wildtype retinas at P7. **(H)** Two-hour, 30-hour and 60-hour EdU pulse-chase of P0 RPCs overexpressing *Zfp292* in retina explants. Mean ± SD (n=4, ***P< 0.001; Two tailed Student's T test). *CAG-filler*: filler plasmid DNA to ensure the equivalent plasmid concentrations. **(I)** m^6A peaks on the *Cdkn1a* gene in wildtype retinas at P7. **(J)** $P21^{Cip1}$ (encoded by the *Cdkn1a* gene) staining in control and Mettl14-cKO retinas at P7. Scale bar: 20μm.

Figure 5

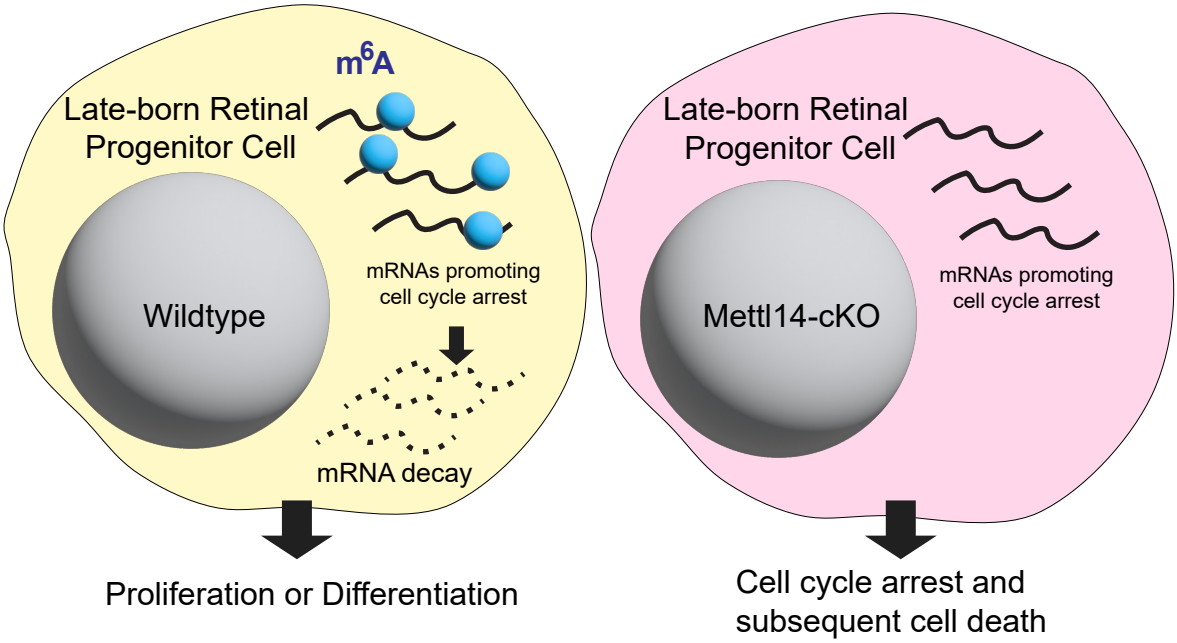
m6A
Late-born Retinal Progenitor Cell
Wildtype
mRNAs promoting cell cycle arrest
mRNA decay
Proliferation or Differentiation
Late-born Retinal Progenitor Cell
Mettl14-cKO
mRNAs promoting cell cycle arrest
Cell cycle arrest and subsequent cell death

Figure 5. The working model for how late-born RPCs counter the cell cycle lengthening during retinal development

Under wildtype conditions, the mRNAs promoting cell cycle arrest, such as *Zfp292*, are modified by m^6A, which decreases their mRNA levels to avoid uncontrolled cell cycle arrest. In the absence of m^6A, these mRNAs are more stable, resulting in cell cycle arrest and the subsequent cell death of late-born RPCs.